Computational and Experimental Investigation of Ti Substitution in Li 1 (Ni x Mn x Co 1−2x−y Ti y)O 2 for Lithium Ion Batteries

ARTICLE *in* JOURNAL OF PHYSICAL CHEMISTRY LETTERS · OCTOBER 2014

Impact Factor: 7.46 · DOI: 10.1021/jz5017526

5 AUTHORS, INCLUDING:

Isaac Markus
University of California, Berkeley
13 PUBLICATIONS **98** CITATIONS
SEE PROFILE

Feng Lin
Lawrence Berkeley National Laboratory
40 PUBLICATIONS **321** CITATIONS
SEE PROFILE

Marca M. Doeff
Lawrence Berkeley National Laboratory
154 PUBLICATIONS **2,976** CITATIONS
SEE PROFILE

THE JOURNAL OF PHYSICAL CHEMISTRY Letters

Letter

pubs.acs.org/JPCL

Computational and Experimental Investigation of Ti Substitution in $Li_1(Ni_xMn_xCo_{1-2x-y}Ti_y)O_2$ for Lithium Ion Batteries

Isaac M. Markus,*[,†,‡] Feng Lin,[‡] Kinson C. Kam,[¶] Mark Asta,[†,§] and Marca M. Doeff*[,‡]

[†]Materials Science and Engineering Department, University of California Berkeley, Berkeley, California 94720, United States

[‡]Environmental Energy Technologies Division and [§]Materials Science Division, Lawrence Berkeley National Lab, Berkeley, California 94720, United States

[¶]Haldor Topsøe A/S, Nymø llevej 55, 2800 Kongens Lyngby, Denmark

Supporting Information

ABSTRACT: Aliovalent substitutions in layered transition-metal cathode materials has been demonstrated to improve the energy densities of lithium ion batteries, with the mechanisms underlying such effects incompletely understood. Performance enhancement associated with Ti substitution of Co in the cathode material $Li_1(Ni_xMn_xCo_{1-2x})O_2$ were investigated using density functional theory calculations, including Hubbard-U corrections. An examination of the structural and electronic modifications revealed that Ti substitution reduces the structural distortions occurring during delithiation due to the larger cation radius of Ti^{4+} relative to Co^{3+} and the presence of an electron polaron on Mn cations induced by aliovalent Ti substitution. The structural differences were found to correlate with a decrease in the lithium intercalation voltage at lower lithium concentrations, which is consistent with quasi-equilibrium voltages obtained by integrating data from stepped potential experiments. Further, Ti is found to suppress the formation of a secondary rock salt phase at high voltage. Our results provide insights into how selective substitutions can enhance the performance of cathodes, maximizing the energy density and lifetime of current Li ion batteries.

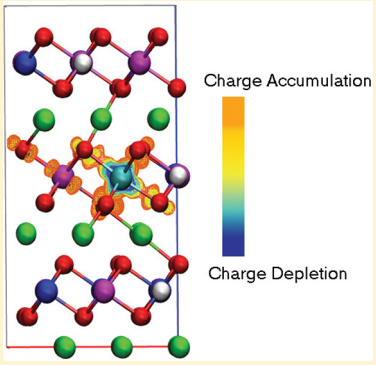

SECTION: Energy Conversion and Storage; Energy and Charge Transport

Understanding the physicochemical origin of material performance in energy conversion and storage applications has allowed for breakthroughs in numerous applications. In the fields of photovoltaics, fuel cells, and batteries, significant improvements have been achieved through combined experimental and computational material design from the atomic to continuum scale.[1−3] This approach has been particularly successful in Li ion batteries, where the research and development advances have facilitated the portable electronic revolution of the last 2 decades. More recently, the improvements in energy density, performance, and manufacturing, have permitted commercial endeavors to be taken for grid storage and transportation applications. In order to further enable Li ion batteries for these newer applications and properly leverage the expertise and manufacturing investments already made, additional improvements in cost, lifetime, and power density are required.[4,5] The class of stoichiometric layered compounds $Li_1(Ni_xMn_xCo_{1-2x})O_2$ known as NMCs, illustrated in Figure 1, are attractive cathode materials for Li ion batteries due to the high rate capability, high capacity, reduced Co content compared to $LiCoO_2$, and superior structural stability relative to lithium-rich compounds.[6−9] Recently, NMCs have been reported to exhibit enhanced performance when Ti^{4+} substitutes Co^{3+} by 2−4%,[10] exhibiting better first cycle Coulombic efficiency, increased capacity, and enhanced cycling stability. Some of these improvements have also been reported for NMCs containing less than 5% of La, Ce, Pr, Mo, or Al[11−16] as well as in doped $LiFePO_4$ and $LiMn_2O_4$.[17−19] Collectively,

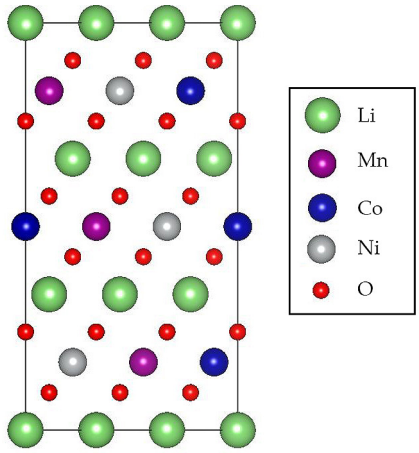

Figure 1. Computational model of the crystal structure of NMC with space group $P3_112$.

Received: August 19, 2014
Accepted: October 4, 2014
Published: October 9, 2014

   dx.doi.org/10.1021/jz5017526 | J. Phys. Chem. Lett. 2014, 5, 3649−3655

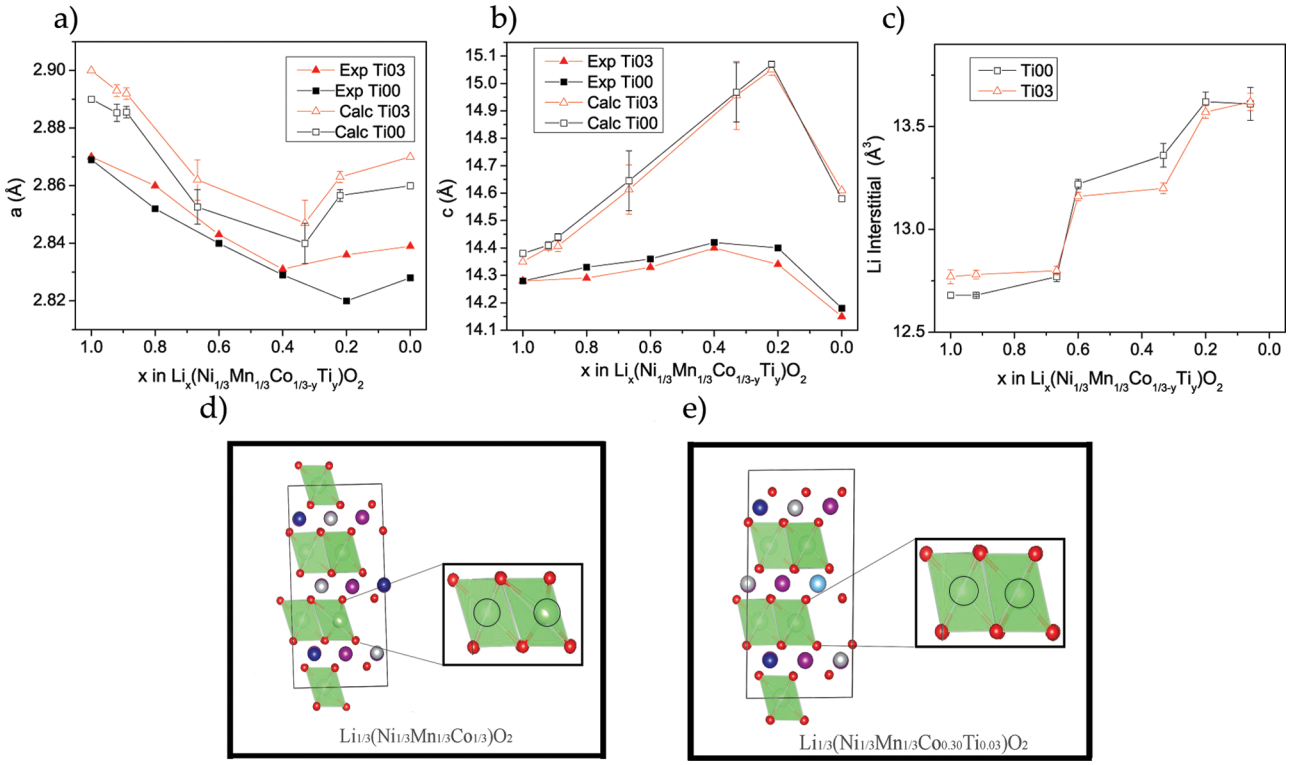

Figure 2. (a,b) Experimental and calculated changes in *a* and *c* lattice parameters as a function of lithium concentration for unsubstituted and Ti-substituted NMCs. Experimental data was taken from Kam et al.[10] and is labeled Exp Ti00 or Exp Ti03 for unsubstituted and Ti-substituted NMCs, respectively. The calculated lattice parameters are labeled Calc Ti00 and Calc Ti03 for unsubstituted and Ti-substituted NMCs, respectively. (c) Changes in the Li interstitial volume. (d,e) Oxygen octahedra around lithium cations after 2/3 of lithium has been removed for unsubstituted and Ti-substituted NMCs. In panels (a)−(c), the error bars denote the standard error in the mean value averaged over five different randomly generated configurations for lithium at each concentration.

these results demonstrate the capability of tuning electrode performance by selective atomic substitutions. For this strategy to be successfully implemented, the exact mechanism by which such improvements occur should be better understood, which requires detailed investigations into the ways in which substitutions affect the properties of the system.[11]

In this Letter, we consider the correlation between electronic and structural changes achieved by small (<5%) Ti substitution of Co in NMCs and the subsequent impact on thermodynamic properties in the context of improved cell performance. We present a general design criteria for improving Li ion cell performance by selective substitution, which can be further extended to a wide set of electrochemical applications. By employing density functional theory (DFT) calculations, we show how the local structural distortions generated through Ti substitution at different lithium concentrations affect the lithium intercalation voltage and the formation energy of a secondary rock salt structure. We find that Ti decreases overall changes in the lithium interstitial volume during cycling, which coincides with a decrease in the intercalation voltages at the lower lithium concentrations. Furthermore, we find that Ti substitution suppresses the formation of a secondary rock salt phase, which has recently been shown to increase the overall battery impedance, leading to capacity fading when cycling to voltages above 4.5 V at constant C rates.[20] This finding can be significant for other cathode systems that undergo similar electrochemically activated transformations at high voltages. One such case is seen for the Li_2MnO_3 structure, which is believed to be the component of the high-capacity Li-rich composite cathodes[21] active beyond 4.4 V. These materials undergo a structural transformation of the layered component, where concomitant removal of Li and O during the formation cycle results in voltage fading that affects their overall power density.

To investigate the effect of Ti substitution on NMCs, we considered the different experimental results observed and provided insights derived from electronic structure calculations based on DFT with Hubbard-U corrections. We first considered the structural changes that occur during delithiation of the NMC structure. Experimentally, Ti substitution is found to lead to a smaller decrease in the overall volume change during cell cycling relative to the unsubstituted material.[10] The smaller volume change during cycling should provide added structural stability, particularly when charging to high voltage (4.7 V versus Li^+/Li). Figure 2a and b shows the calculated change in the lattice parameters during lithium removal along with experimental measurements taken from Kam et al.[10] The calculations reproduce the experimental trends in that Ti substitution reduces the change in the *a* parameter at lower Li content while not significantly affecting the change in the *c* parameter. The large error bars for the intermediate values of *x* in Figure 2a and b originate from a limited sampling of the configurational order. A more sophisticated treatment, accounting properly for short-range ordering effects, lies beyond the scope of the present work due to the large number of components. Nevertheless, the variation in the calculated lattice parameters with the configurations sampled was relatively small for Li contents near zero and one (as indicated by the smaller error bars), and thus, the main findings concerning the effect of Ti on the lattice parameters at lower Li

dx.doi.org/10.1021/jz5017526 | J. Phys. Chem. Lett. 2014, 5, 3649−3655

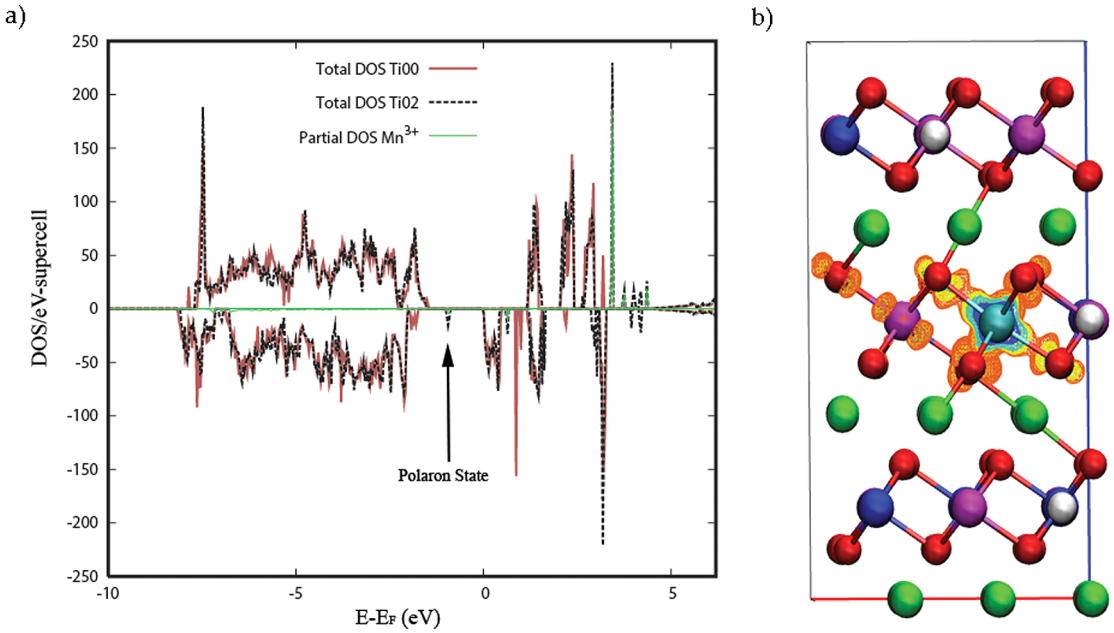

Figure 3. Localized polaron by plotting (a) the total density of states (DOS) for unsubstituted NMC (red line) and Ti-substituted NMC (black line), including the projected DOS for the Mn^{3+} cation (green line). (b) The charge density difference map between unsubstituted and Ti-substituted NMCs. The colored spheres indicate green for Li, red for O, blue for Co, white for Ni, and purple for Mn. The colored bands represent charge depletion for the blue bands and charge accumulation for yellow and orange bands.

content are considered robust. Furthermore, general agreement between computation and experimental results supports the finding that the lithium interstitial volume undergoes a smaller change in the Ti-substituted structure, as shown in Figure 2c. The interstitial volume was calculated using the algorithm of Swanson and Peterson,[22] as implemented in the VESTA molecular viewer software.[23] Changes to the lithium interstitial volume have been previously related to the mobility of lithium in the NMC structure,[16] which is related to the overall stability of lithium in the structure. Figure 2d and 2e shows the MO_6 octahedron around each lithium after two-thirds of the lithium have been removed from the structure and illustrates distortions in the regular NMC compared to the Ti-substituted structure.

Our calculations show that the structural differences can be attributed first to the substitution of Co^{3+} with the larger Ti^{4+} cation, which expands the surrounding MO_6 octahedra, and second to the formation of a charge-compensating electron polaron on a nearby Mn^{3+} (Figure 3) that also expands the surrounding MO_6 octahedra. These two new structural features evolve differently once lithium is removed. As expected, the distortions around the Ti cation persist because Ti^{4+} is electrochemically inactive, while the electron polaron will oxidize once lithium is removed. However, because aliovalent substitution provides an extra electron, for a given delithiation amount, we find fewer of the Ni/Co redox centers fully oxidized, which aids in volume preservation. Table 1 shows the average bond length between oxygen and each transition metal for their different oxidation states. As expected, the more oxidized species have shorter bonds, which combined with the larger Ti cation size, results in a decrease of structural changes during cycling. Although increasing the Ti content should stabilize the structure even more, experimental results[10] indicate that performance deteriorates at substitution levels in excess of 5% as impurity phases begin to form, revealing a practical limit for substitutions.

Table 1. Average Calculated O−M Bond Lengths

metal−O	average bond length (Å)
Mn^{3+}−O	1.98
Mn^{4+}−O	1.93
Ni^{2+}−O	2.07
Ni^{3+}−O	1.92
Ni^{4+}−O	1.88
Co^{3+}−O	1.93
Co^{4+}−O	1.89
Ti^{4+}−O	1.96

The intercalation voltage was calculated for the unsubstituted and Ti-substituted NMCs, and we found that the average voltage decreased for the substituted compound. This finding was confirmed experimentally; Figure 4a shows the integrated data from a stepped potential experiment. This figure indicates that under quasi-equilibrium conditions, Ti substitution lowers the intercalation voltage. Figure 4b shows the voltage differences between unsubstituted NMC and Ti-substituted NMC as determined experimentally and computationally. Both sets of results show that the voltage shifts to lower values in the Ti-substituted sample for low and high Li contents and is unchanged for intermediate values. Although the calculations consider only a limited number of concentrations, they are seen to produce results that agree with the experimental results in terms of the trends with Li content and the overall magnitude of the Ti-induced potential shift. This lower equilibrium potential reduces the overpotential required to drive lithium deintercalation, allowing more lithium to be accessed, providing an explanation for the increased capacity found experimentally. These results are analogous to previous findings that through Fe addition to NMC, the intercalation voltage can be raised.[11] These observations demonstrate the capability for tuning electrode performance by manipulating the voltage of NMCs in order to deliver superior energy density for batteries.

dx.doi.org/10.1021/jz5017526 | J. Phys. Chem. Lett. 2014, 5, 3649−3655

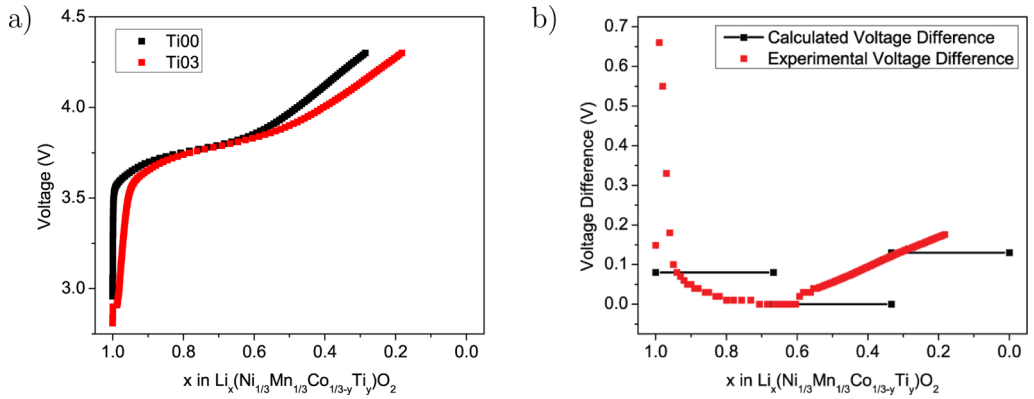

Figure 4. (a) Experimental quasi-equilibrium voltage for unsubstituted NMC (black squares) and Ti-substituted NMC (red squares) by integrating data from a stepped potential experiment. (b) Voltage difference between the intercalation voltage for unsubstituted and Ti-substituted NMCs as calculated using DFT (black curve) and experimentally using the stepped potential experiment (red curve).

Another contributing factor for the increased capacity found experimentally comes from the improved first cycle Coulombic efficiency and decreased discharge capacity fading when cells are charged to high voltages (>4.3 V).[10] At high states of charge, there are multiple side reactions contributing to Coulombic inefficiencies in lithium ion batteries, including oxygen evolution,[24,25] electrolyte decomposition,[26,27] and surface reconstructions.[6,20,28] A phase transformation that impacts performance is the surface reconstruction from the layered NMC structure to a rock salt oxide.[20] For this transformation to occur, an initial amount of oxygen and lithium must be lost, contributing to the first cycle Coulombic inefficiency, with subsequent high-voltage cycles removing small amounts of active material that continue to build up this high impedance secondary phase, resulting in accelerated capacity fading. Figure 5 compares the free-energy change at room temperature for the formation of the rock salt structure from the NMC (see eq 1 in the Computational Methods section) at different lithium concentrations for the unsubstituted and Ti-substituted NMCs. The calculated results indicate that Ti helps stabilize the NMC structure by increasing the energy of formation of the rock salt structure and more strongly binding oxygen. This result agrees with previous reports that Ti has higher O binding energy compared to the other metals in NMC and offsets oxygen depletion to higher states of charge.[29,30] Shifting the energy of formation by Ti substitution allows for more of the capacity of the NMC to be used toward the reversible intercalation of Li, rather than the irreversible oxygen evolution and surface reconstruction.

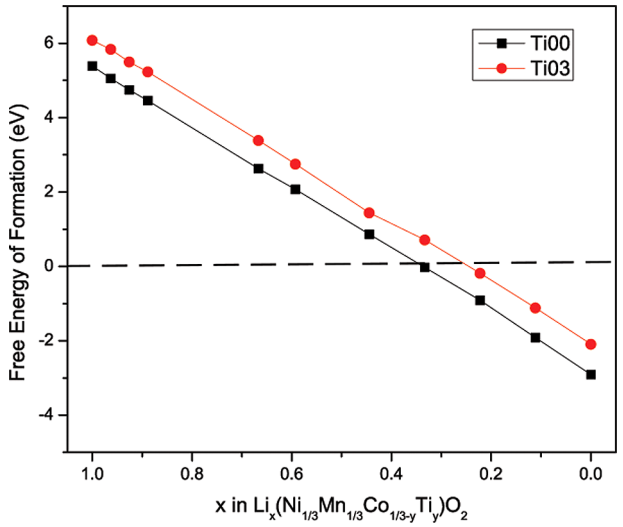

Figure 5. Calculated free energy of formation at room temperature for the rock salt structure from NMC structures with different lithium concentrations. The black line (Ti00) corresponds to unsubstituted NMC, and the red line (Ti03) corresponds to Ti-substituted NMC.

The calculations performed not only help identify the role that Ti has on the performance of NMC cathodes but suggests important selection criteria for substituting cations in order to tune the properties of layered cathode materials. To decrease the lithium intercalation voltage, (i) substituting cations should have larger ionic radii in order to decrease the lithium interstitial volume. (ii) In case the substitutional cation is electrochemically inactive, aliovalent substitutions that result in the formation on an electron polaron will also decrease changes to the lithium interstitial volume during delithiation. The main reason for reducing the lithium interstitial voltage is so that more lithium can be accessed for a given experimental overpotential. Alternatively, increasing the lithium interstitial volume by using smaller cations such as Al^{3+} will increase the intercalation voltage; use of such substitutional cations thus requires the development of novel electrolytes that will not oxidize at high voltages. (iii) Substituting cations should also have stronger oxygen binding in order to improve phase stability during cycling. By suppressing oxygen loss and the formation of high impedance phases, discharge fading can be mitigated, prolonging not only battery life but also energy density. It is worth noting that this design criteria extends beyond cathodes for Li ion batteries and can be applied to a wide range of intercalation compounds used in other energy storage chemistries, including emerging Na and Mg ion batteries, as well as primary alkaline batteries. Furthermore, intercalation processes are important not only for lithium batteries but for other types of devices as well, such as electrochromics, where selective substitutions have also been shown to improve durability and switching kinetics.[31,32]

COMPUTATIONAL METHODS

DFT calculations were performed with the projector augmented wave (PAW) method,[33,34] as implemented in the Vienna ab initio simulation package (VASP).[35,36] The calculations made use of the spin-dependent generalized gradient approximation of Perdew, Burke, and Ernzerhof

dx.doi.org/10.1021/jz5017526 | J. Phys. Chem. Lett. 2014, 5, 3649−3655

(PBE),[37] including Hubbard-U corrections following the formalism developed by Dudarev et al.[38] The electron states were sampled using a k-point grid of 2 × 2 × 2 centered at the origin. The electronic wave functions were expanded in a plane wave basis set with an energy cutoff of 600 eV, and the ionic positions were optimized until the forces on the ions were converged to 10 meV/Å. The values for the Hubbard-U parameters for Ni, Mn, and Co were initially determined from previous computational work on Li intercalation compounds[39] and subsequently optimized by iteratively calculating lithium intercalation voltage profiles that also exhibit the order of oxidation previously reported in the literature of Ni^{2+}/Ni^{3+}, Ni^{3+}/Ni^{4+}, and Co^{3+}/Co^{4+}.[11,40] The final values used for the calculations were 7.0, 5.0, and 5.5 eV for Ni, Mn, and Co, respectively. The oxidation order was determined by calculating the oxidation state of each ion by integrating the local magnetic moment as calculated by VASP at 100, 66, 33, and 0% lithium concentration. An exact match for the experimental intercalation voltage was not possible due to the limited number of configurations sampled and the fact that calculated voltages were based on energies alone. A more sophisticated treatment would require the development of a model for configurational thermodynamic properties, including short-range-ordering effects and the inclusion of configurational and electronic entropy contributions to the free energy. Such a computational thermodynamic approach lies beyond the scope of the present work due to the large number of components involved in the NMC materials.

The calculations for NMC compounds made use of a supercell geometry containing 27 formula units (see Figure 1) and a space group $P3_112$.[41] This structure exhibits a local ordering of the transition metals and thus a lower symmetry than the $R\bar{3}m$ space group, corresponding to a disordered solid solution. The supercell model was selected in order to minimize the number of different structural arrangements in the metal layer, with the additional consideration that the periodic boundary conditions would also create an ordered system. The impact of the supercell geometry was checked by generating an additional structure that had equal distribution of each transition metal by layer but with local ordering generated only by the periodic boundary conditions. Lithium transport effects were not consider in this work, but previous work in the literature[42−46] suggests that consideration of the local ordering effects can have a significant impact on calculated intercalation kinetics. Further, it has been shown that changes in cation order can impact intercalation voltages,[47] and such effects in NMC materials will be discussed in future studies. We found that lattice parameter changes and lithium intercalation values did not significantly change, with the results falling within the standard errors in the mean reported. Structural parameter changes and lithium intercalation voltage differences were calculated at each lithium concentration by averaging over five structures with different lithium arrangements for unsubstituted and substituted NMC. The five arrangements were generated by randomly removing equal amounts of lithium from each lithium layer.

In order to determine the relative stability of the layered versus rock salt structure, the reaction free energy was calculated for the following reaction at different initial lithium concentrations.

$$2\mathrm{Li}_x(\mathrm{Ni}_{1/3}\mathrm{Co}_{1/3-y}\mathrm{Mn}_{1/3}\mathrm{Ti}_y)\mathrm{O}_2 \rightarrow 2(\mathrm{Ni}_{1/3}\mathrm{Co}_{1/3-y}\mathrm{Mn}_{1/3}\mathrm{Ti}_y)\mathrm{O} + \mathrm{O}_2 + 2x\mathrm{Li} \quad (1)$$

where the first term represents the NMC structure previously described, followed by the rock salt structure (space group $Fm\bar{3}m$), which is also modeled with a supercell containing 27 formula units with the same transition-metal arrangement as the layered structure. The last two terms correspond to the oxygen dimer and bcc lithium metal, respectively. The Gibbs free energy for solid species was approximated by the zero-temperature energies, neglecting vibrational contributions and assuming that the configuration disorder in the Ni, Co, and Mn sublattices is frozen in at the temperatures of interest. For the oxygen molecule, the Gibbs free energy was computed using a standard ab initio thermodynamics formalism, in which the free energy is decomposed into three parts, (i) a zero-temperature energy calculated from DFT and corrected by an overbinding error, as described by Wang et al.,[48] (ii) the zero-point energy of the oxygen molecule, (iii) finite-temperature contributions arising from vibrational, translational, and orientational motion and taken from experimental measurements corresponding to a temperature of 298 K and a partial pressure of 1 atm, and (iv) a term $RT\ln(p_{O_2})$ to account for variations of the oxygen partial pressure of 10^{-6} atm. The low partial pressure was selected to simulate typical oxygen concentrations during battery cell assembly, approximately 0.5 ppm.

EXPERIMENTAL METHODS

$\mathrm{Li}_1(\mathrm{Ni}_{0.33}\mathrm{Mn}_{0.33}\mathrm{Co}_{0.33-y}\mathrm{Ti}_y)\mathrm{O}_2$ compounds were synthesized by the glycine nitrate combustion process described by Kam et al.[10] To prepare electrodes, the active material was mixed with polyvinylidene fluoride (PVdF, Kureha Chemical Ind. Co. Ltd.), acetylene black (Denka, 50% compressed), and SFG-6 synthetic graphite (Timcal Ltd., Graphites and Technologies) in the ratio 84:8:4:4 in N-methyl-2-pyrrolidinone to make a slurry. Once homogenized, the slurry was cast onto a carbon-coated Al foil current collector (Exopack Advanced Coatings) and dried in air and under vacuum at 120 °C for 12 h. Electrodes were then cut to size, and 2032 coin cells were assembled using Celgard 3401 soaked with a solution of 1 M $LiPF_6$ in 1:2 ethylene carbonate/dimethyl carbonate (EC-DMC, Ferro Corp.) as the electrolytic solution and lithium foils as anodes. Slow stepped potential experiments were carried out on a MacPile II (Biologic, S.A., Claix, France) galvanostat/potentiostat. For these experiments, 10 mV potential steps were used, and the next step was taken when the current fell to 1/60000 of the initial value or an absolute value of 0.008 mA, whichever came first. This was equivalent to a rate of approximately °C/100 (removal of one lithium per formula unit in 100 h). Data were integrated to produce the quasi-equilibrium V versus x curves shown in Figure 4.

ASSOCIATED CONTENT

Supporting Information

Determination of Hubbard-U parameter values. This material is available free of charge via the Internet at http://pubs.acs.org.

AUTHOR INFORMATION

Corresponding Authors

*E-mail: isaac.markus@berkeley.edu (I.M.M.).
*E-mail: mmdoeff@lbl.gov (M.D.).

Notes

The authors declare no competing financial interest.

■ ACKNOWLEDGMENTS

This work was supported by the Assistant Secretary for Energy Efficiency and Renewable Energy, Office of Vehicle Technologies of the U.S. Department of Energy under Contract No. DE-AC02-05CH11231 under the Batteries for Advanced Transportation Technologies (BATT) Program. This work made use of computational resources provided by the National Energy Research Supercomputer Center (NERSC), which is supported by the Office of Science of the U.S. Department of Energy under Contract DE-AC03-76SF00098. This work also used the Extreme Science and Engineering Discovery Environment (XSEDE), which is supported by National Science Foundation Grant Number ACI-1053575. I.M.M acknowledges the support of the NSF graduate research fellowship program and Dr. Kristin Persson for useful discussions and feedback.

■ REFERENCES

(1) Rhle, S.; Anderson, A. Y.; Barad, H.-N.; Kupfer, B.; Bouhadana, Y.; Rosh-Hodesh, E.; Zaban, A. All-Oxide Photovoltaics. *J. Phys. Chem. Lett.* **2012**, *3*, 3755−3764.

(2) Swider-Lyons, K. E.; Campbell, S. A. Physical Chemistry Research toward Proton Exchange Membrane Fuel Cell Advancement. *J. Phys. Chem. Lett.* **2013**, *4*, 393−401.

(3) Erickson, E. M.; Ghanty, C.; Aurbach, D. New Horizons for Conventional Lithium Ion Battery Technology. *J. Phys. Chem. Lett.* **2014**, *5*, 3313−3324.

(4) Armand, M.; Tarascon, J.-M. Building Better Batteries. *Nature* **2008**, *451*, 652−657.

(5) Goodenough, J. B.; Kim, Y. Challenges for Rechargeable Li Batteries. *Chem. Mater.* **2010**, *22*, 587−603.

(6) Martha, S.; Markevich, E.; Burgel, V.; Salitra, G.; Zinigrad, E.; Markovsky, B.; Sclar, H.; Pramovich, Z.; Heik, O.; Aurbach, D.; Exnar, I.; Buqa, H.; Drezen, T.; Semrau, G.; Schmidt, M.; et al. A Short Review on Surface Chemical Aspects of Li Batteries: A Key for a Good Performance. *J. Power Sources* **2009**, *189*, 288−296.

(7) Yoon, W.-S.; Chung, K. Y.; McBreen, J.; Yang, X.-Q. A Comparative Study on Structural Changes of $LiCo_{1/3}Ni_{1/3}Mn_{1/3}O_2$ and $LiNi_{0.8}Co_{0.15}Al_{0.05}O_2$ during First Charge Using in Situ XRD. *Electrochem. Commun.* **2006**, *8*, 1257−1262.

(8) Whitfield, P.; Davidson, I.; Cranswick, L.; Swainson, I.; Stephens, P. Investigation of Possible Superstructure and Cation Disorder in the Lithium Battery Cathode Material $LiCo_{1/3}Ni_{1/3}Mn_{1/3}O_2$ Using Neutron and Anomalous Dispersion Powder Diffraction. *Solid State Ionics* **2005**, *176*, 463−471.

(9) Pan, C.; Banks, C. E.; Song, W.; Wang, C.; Chen, Q.; Ji, X. Recent Development of $LiNi_xCo_yMn_zO_2$: Impact of Micro/Nano Structures for Imparting Improvements in Lithium Batteries. *Trans. Nonferrous Met. Soc. China* **2013**, *23*, 108−119.

(10) Kam, K. C.; Mehta, A.; Heron, J. T.; Doeff, M. M. Electrochemical and Physical Properties of Ti-Substituted Layered Nickel Manganese Cobalt Oxide (NMC) Cathode Materials. *J. Electrochem. Soc.* **2012**, *159*, A1383−A1392.

(11) Meng, Y. S.; Wu, Y. W.; Hwang, B. J.; Li, Y.; Ceder, G. Combining Ab Initio Computation with Experiments for Designing New Electrode Materials for Advanced Lithium Batteries: $Li_1Ni_{1/3}Fe_{1/6}Co_{1/6}Mn_{1/3}O_2$. *J. Electrochem. Soc.* **2004**, *151*, A1134−A1140.

(12) Ding, Y.; Zhang, P.; Jiang, Y.; Gao, D. Effect of Rare Earth Elements Doping on Structure and Electrochemical Properties of $LiNi_{1/3}Co_{1/3}Mn_{1/3}O_2$ for Lithium-Ion Battery. *Solid State Ionics* **2007**, *178*, 967−971.

(13) Liu, D.; Wang, Z.; Chen, L. Comparison of Structure and Electrochemistry of Al- and Fe-Doped $LiNi_{1/3}Co_{1/3}Mn_{1/3}O_2$. *Electrochim. Acta* **2006**, *51*, 4199−4203.

(14) Wang, L. Q.; Jiao, L. F.; Yuan, H.; Guo, J.; Zhao, M.; Li, H. X.; Wang, Y. M. Synthesis and Electrochemical Properties of Mo-Doped $Li(Ni_{1/3}Mn_{1/3}Co_{1/3})O_2$ Cathode Materials for Li-Ion Battery. *J. Power Sources* **2006**, *162*, 1367−1372.

(15) Wilcox, J. D.; Rodriguez, E. E.; Doeff, M. M. The Impact of Aluminum and Iron Substitution on the Structure and Electrochemistry of $Li(Ni_{0.4}Co_{0.2-y}M_yMn_{0.4})O_2$ Materials. *J. Electrochem. Soc.* **2009**, *156*, A1011−A1018.

(16) Wilcox, J.; Patoux, S.; Doeff, M. Structure and Electrochemistry of $LiNi_{1/3}Co_{1/3-y}M_yMn_{1/3}O_2$ (M=Ti,Al,Fe) Positive Electrode Materials. *J. Electrochem. Soc.* **2009**, *156*, A192−A198.

(17) Van der Ven, A.; Ceder, G. Ordering in $Li_x(Ni_{0.5}Mn_{0.5})O_2$ and Its Relation to Charge Capacity and Electrochemical Behavior in Rechargeable Lithium Batteries. *Electrochem. Commun.* **2004**, *6*, 1045−1050.

(18) Shi, S.; Wang, D.; Meng, S.; Chen, L.; Huang, X. First-Principles Studies of Cation-Doped Spinel $LiMn_2O_4$ for Lithium Ion Batteries. *Phys. Rev. B* **2003**, *67*, 115130.

(19) Wu, G.; Wu, S.; Wu, P. Doping-Enhanced Lithium Diffusion in Lithium-Ion Batteries. *Phys. Rev. Lett.* **2011**, *107*, 118302.

(20) Lin, F.; Markus, I. M.; Nordlund, D.; Weng, T.-C.; Asta, M. D.; Xin, H. L.; Doeff, M. M. Surface Reconstruction and Chemical Evolution of Stoichiometric Layered Cathode Materials for Lithium-Ion Batteries. *Nat. Commun.* **2014**, *5*, 3529.

(21) Lee, E.; Persson, K. A. Structural and Chemical Evolution of the Layered Li-Excess Li_xMnO_3 as a Function of Li Content from First-Principles Calculations. *Adv. Energy Mater.* **2014**, 1400498−1400506.

(22) Swanson, D. K.; Peterson, R. C. Polyhedral Volume Calculations. *Can. Mineral.* **1980**, *18*, 153−156.

(23) Momma, K.; Izumi, F. *VESTA*: a Three-Dimensional Visualization System for Electronic and Structural Analysis. *J. Appl. Crystallogr.* **2008**, *41*, 653−658.

(24) Armstrong, A. R.; Holzapfel, M.; Novk, P.; Johnson, C. S.; Kang, S.-H.; Thackeray, M. M.; Bruce, P. G. Demonstrating Oxygen Loss and Associated Structural Reorganization in the Lithium Battery Cathode $Li(Ni_{0.2}Li_{0.2}Mn_{0.6})O_2$. *J. Am. Chem. Soc.* **2006**, *128*, 8694−8698.

(25) Lu, Z.; Dahn, J. R. Understanding the Anomalous Capacity of $Li/Li(Ni_xLi_{(1/3-2x/3)}Mn_{(2/3-x/3)})O_2$ Cells Using in Situ X-ray Diffraction and Electrochemical Studies. *J. Electrochem. Soc.* **2002**, *149*, A815−A822.

(26) Niehoff, P.; Passerini, S.; Winter, M. Interface Investigations of a Commercial Lithium Ion Battery Graphite Anode Material by Sputter Depth Profile X-ray Photoelectron Spectroscopy. *Langmuir* **2013**, *29*, 5806−5816.

(27) Andersson, A. M.; Abraham, D. P.; Haasch, R.; MacLaren, S.; Liu, J.; Amine, K. Surface Characterization of Electrodes from High Power Lithium-Ion Batteries. *J. Electrochem. Soc.* **2002**, *149*, A1358−A1369.

(28) Xu, B.; Fell, C. R.; Chi, M.; Meng, Y. S. Identifying Surface Structural Changes in Layered Li-Excess Nickel Manganese Oxides in High Voltage Lithium Ion Batteries: A Joint Experimental and Theoretical Study. *Energy Environ. Sci.* **2011**, *4*, 2223−2233.

(29) Xiao, P.; Deng, Z. Q.; Manthiram, A.; Henkelman, G. Calculations of Oxygen Stability in Lithium-Rich Layered Cathodes. *J. Phys. Chem. C* **2012**, *116*, 23201−23204.

(30) Choi, J.; Manthiram, A. Role of Chemical and Structural Stabilities on the Electrochemical Properties of Layered $Li-Co_{1/3}Ni_{1/3}Mn_{1/3}O_2$ Cathodes. *J. Electrochem. Soc.* **2005**, *152*, A1714−A1718.

(31) Fang, W. Q.; Gong, X.-Q.; Yang, H. G. On the Unusual Properties of Anatase TiO_2 Exposed by Highly Reactive Facets. *J. Phys. Chem. Lett.* **2011**, *2*, 725−734.

(32) Lin, F.; Cheng, J.; Engtrakul, C.; Dillon, A. C.; Nordlund, D.; Moore, R. G.; Weng, T.-C.; Williams, S. K. R.; Richards, R. M. In Situ Crystallization of High Performing WO_3-Based Electrochromic Materials and the Importance for Durability and Switching Kinetics. *J. Mater. Chem.* **2012**, *22*, 16817−16823.

(33) Blöchl, P. E. Projector Augmented-Wave Method. *Phys. Rev. B* **1994**, *50*, 17953−17979.
(34) Kresse, G.; Joubert, D. From Ultrasoft Pseudopotentials to the Projector Augmented-Wave Method. *Phys. Rev. B* **1999**, *59*, 1758−1775.
(35) Kresse, G.; Furthmüller, J. Efficient Iterative Schemes for Ab-Initio Total-Energy Calculations Using a Plane-Wave Basis Set. *Phys. Rev. B* **1996**, *54*, 11169−11186.
(36) Kresse, G.; Furthmüller, J. Efficiency of Ab-Initio Total Energy Calculations for Metals and Semiconductors Using a Plane-Wave Basis Set. *Comput. Mater. Sci.* **1996**, *6*, 15−50.
(37) Perdew, J. P.; Burke, K.; Ernzerhof, M. Generalized Gradient Approximation Made Simple. *Phys. Rev. Lett.* **1997**, *78*, 1396−1396.
(38) Dudarev, S. L.; Botton, G. A.; Savrasov, S. Y.; Humphreys, C. J.; Sutton, A. P. Electron-Energy-Loss Spectra and the Structural Stability of Nickel Oxide. *Phys. Rev. B* **1998**, *57*, 1505−1509.
(39) Zhou, F.; Cococcioni, M.; Marianetti, C.; Morgan, D.; Ceder, G. First-Principles Prediction of Redox Potentials in Transition-Metal Compounds with LDA+U. *Phys. Rev. B* **2004**, *70*, 235121.
(40) Hwang, B. J.; Tsai, Y. W.; Carlier, D.; Ceder, G. A Combined Computational/Experimental Study on $LiNi_{1/3}Co_{1/3}Mn_{1/3}O_2$. *Chem. Mater.* **2003**, *15*, 3676−3682.
(41) Koyama, Y.; Yabuuchi, N.; Tanaka, I.; Adachi, H.; Ohzuku, T. Solid-State Chemistry and Electrochemistry of $LiCo_{1/3}Ni_{1/3}Mn_{1/3}O_2$ for Advanced Lithium-Ion Batteries. *J. Electrochem. Soc.* **2004**, *151*, A1545−A1551.
(42) Kuganathan, N.; Islam, M. S. Li_2MnSiO_4 Lithium Battery Material: Atomic-Scale Study of Defects, Lithium Mobility, and Trivalent Dopants. *Chem. Mater.* **2009**, 5196−5202.
(43) Zhang, P.; Li, X. D.; Yu, S.; Wu, S. Q.; Zhu, Z. Z.; Yang, Y. Effects of Na Substitution on Li Ion Migration in Li_2CoSiO_4 Cathode Material. *J. Electrochem. Soc.* **2013**, *160*, A658−A661.
(44) Mueller, T.; Jain, A.; Ceder, G. Evaluation of Tavorite-Structured Cathode Materials for Lithium-Ion Batteries Using High-Throughput Computing. *Chem. Mater.* **2011**, 3854−3862.
(45) Tritsaris, G. A.; Zhao, K.; Okeke, O. U.; Kaxiras, E. Diffusion of Lithium in Bulk Amorphous Silicon: A Theoretical Study. *J. Phys. Chem. C* **2012**, 22212−22216.
(46) Gardiner, G. R.; Islam, M. S. Anti-Site Defects and Ion Migration in the $LiFe_{0.5}Mn_{0.5}PO_4$ Mixed-Metal Cathode Material. *Chem. Mater.* **2010**, *22*, 1242−1248.
(47) Lee, E.; Persson, K. a. Revealing the Coupled Cation Interactions Behind the Electrochemical Profile of $Li_xNi_{0.5}Mn_{1.5}O_4$. *Energy Environ. Sci.* **2012**, *5*, 6047−6051.
(48) Wang, L.; Maxisch, T.; Ceder, G. Oxidation Energies of Transition Metal Oxides within the GGA+U Framework. *Phys. Rev. B* **2006**, *73*, 195107.